Journal of Physics: Conference Series **220** (2010) 012015 doi:10.1088/1742-6596/220/1/012015

Open Quantum Dots in Graphene: Scaling Relativistic Pointer States

D K Ferry[1], **L Huang, R Yang, Y-C Lai, R Akis**
School of Electrical, Computer, and Energy Engineering and Center for Solid State Electronics Research, Arizona State University, Tempe, AZ 85287-5706 USA

E-mail: ferry@asu.edu

Abstract. Open quantum dots provide a window into the connection between quantum and classical physics, particularly through the decoherence theory, in which an important set of quantum states are not "washed out" through interaction with the environment—the pointer states provide connection to trapped classical orbits which remain stable in the dots. Graphene is a recently discovered material with highly unusual properties. This single layer, one atom thick, sheet of carbon has a unique bandstructure, governed by the Dirac equation, in which charge carriers imitate relativistic particles with zero rest mass. Here, an atomic orbital-based recursive Green's function method is used for studying the quantum transport. We study quantum fluctuations in graphene and bilayer graphene quantum dots with this recursive Green's function method. Finally, we examine the scaling of the domiant fluctuation frequency with dot size.

1. Introduction

The manner in which the quantum states of a system evolve into their classical counterparts has been of interest since the advent of quantum theory [1]. While dynamical systems may be purely chaotic or regular, the most ubiquitous in nature are those whose phase space is instead *mixed* [2]. The study of quantum behavior in open systems is important, also, to the *decoherence* theory [3]. This latter theory connects the properties of open quantum systems to the existence of a set of *pointer states*, which remain robust in the presence of the environmental coupling, eventually correlating with regular classical orbits. The evidence for such pointer states has been provided in the studies of single open quantum dots [4,5]. And, it has clearly been demonstrated that these quantum states are highly correlated with the classical states that arise in the mixed phase space and satisfy the Kolmogorov-Arnold-Moser behavior [6] expected in such systems [7,8]. It has also been shown that these pointer states exist as families, which include offspring, that lead to periodicities in a magnetic field, and that new states can exist in arrays of quantum dots [9].

Graphene has been the subject of a considerable level of interest in the past few years [10]. This interest seems to originate from the astonishing difference between graphene and other well-known two-dimensional semiconductor systems. This single layer, one atom thick, sheet of carbon has atoms which are arranged into a honeycomb lattice, which produces a unique bandstructure where

[1] To whom any correspondence should be addressed.

the bands and electron transport are mainly derived by the surface normal p_z orbitals. Near the K point, the band structure exhibits a linear energy-momentum relationship, and is effectively described by the Dirac equation, in which charge carriers imitate relativistic particles with zero rest mass. This strictly two-dimensional material exhibits exceptionally high crystalline and electronic quality, and despite its short history, has already revealed an abundance of new physics and potential applications, as well as a very high mobility at room temperature [11,12]. Quantum dots have been described for graphene [13,14], and single-electron charging has been observed in small graphene dots [15,16]. Studies of these dots have shown chaotic behavior [16], but behavior similar to normal semiconductor dots has been found [17]. Importantly, scarring behavior and the tendency to support pointer states has been found in graphene dots which would support chaotic and mixed behavior [18]. Importantly, conduction fluctuations have been suggested [18,19], in keeping with recent experiments in bilayer graphene quantum dots [20].

In this paper, we discuss the computation of conductance through open quantum dots in single-layer and bilayer graphene, using the recursive Green's function formalism. In particular, we discuss the scaling of magnetic field and energy with dot size for the normalized behavior of conductance fluctuations which arise from phase-space tunneling to the pointer states [5]. In the next section, we discuss the properties of graphene and its band structure which are important for these calculations. We then turn to a description of the recursive Green's function technique and its formulation in an atomic basis. Finally, we discuss the observed conductance fluctuations, their dominant characteristics and periods and how these scale with quantum dot size.

2. Graphene

Graphene is a single layer of carbon atoms arranged in a hexagonal honeycomb structure. The proper unit cell contains two atoms per unit cell, which are denoted as atom A and atom B, as shown with two different colors in Fig. 1(a). This leads to an equivalent Brillouin zone with two minima at K and K', as shown in Fig. 1(b). These latter two points are known as the Dirac points for reasons that become clear below. The C-C nearest neighbor distance is a = 0.142 nm, but the length of the primitive lattice vector shown in the figure is 0.246 nm. Carbon atoms possess four valence electrons. Three of these (one s orbital and two p orbital electrons) form tight bonds, known as σ bonds, with three neighboring atoms in the graphene plane. The fourth one is the p_z state, directed normal to the lattice. The σ bonds form a deep valence band which will not play a role in the conductivity. The p_z orbitals form the π band and this constitutes the band of interest. The nature of graphene is such that the most common method of computing the band structure is simple tight-binding, in which both the nearest neighbor interaction and the second-neighbor interactions are important. The former is typically identified by a general matrix element γ_0, while the latter is denoted by the parameter γ_0'. Each atom has 3 nearest neighbors of the opposite type and 6 second neighbors of the same type, and the tight-binding formulation leads to [21]

$$E(\mathbf{k}) = E_0 \pm \gamma_0\sqrt{3 + f(\mathbf{k})} - \gamma_0' f(\mathbf{k})$$
$$f(\mathbf{k}) = 2\cos\left(\sqrt{3}k_y a\right) + 4\cos\left(\frac{\sqrt{3}}{2}k_y a\right)\cos\left(\frac{3}{2}k_x a\right) \quad . \tag{1}$$

This band structure is shown in Fig. 2. At the K and K' points the bands touch. Expanding around these points, for small wave vectors away from these points, we find that the energies are approximately [10]

$$E = E_0 + 3\gamma_0' \pm \frac{3\gamma_0 a}{2}k + O(k^2) \quad . \tag{2}$$

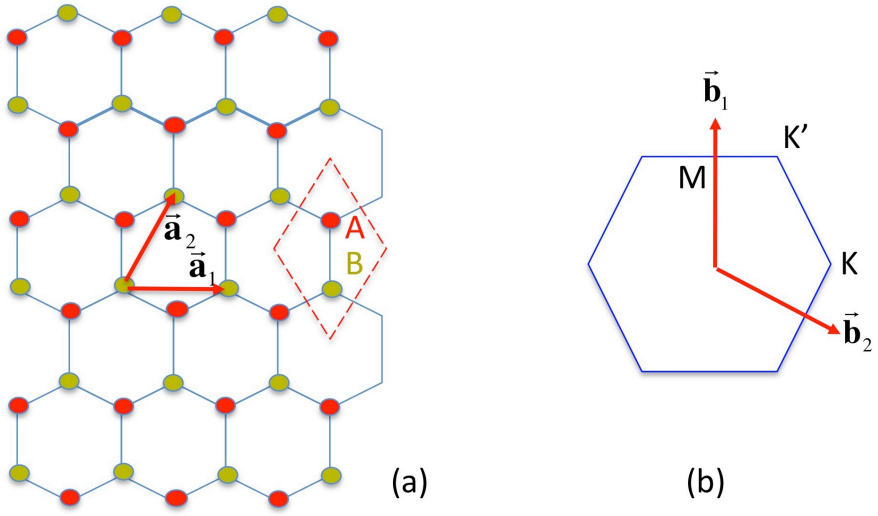

Fig. 1. (a) The hexagonal atomic structure of graphene. The unit cell (dashed line) contains two atoms, denoted as atom A and atom B. Here, the unit vectors are $\mathbf{a}_1 = a(\sqrt{3},0)$, $\mathbf{a}_2 = a(\frac{\sqrt{3}}{2},\frac{3}{2})$, where a = 0.142 nm. (b) The brillouin zone of graphene contains two valleys at K and K'. The reciprocal lattice vectors are $\mathbf{b}_1 = \frac{2\pi}{a}\left(\frac{1}{3},-\frac{1}{\sqrt{3}}\right)$, $\mathbf{b}_2 = \frac{2\pi}{a}\left(0,\frac{2}{3}\right)$.

Without loss of generality, we can set the sum of the first two terms to zero, and then we note that the bands are linear bands, with the upper sign for electrons and the lower sign for holes. Moreover, these bands are chiral, in that the positive slope band has positive helicity and the negative slope band has negative helicity. The helicity arises from the pseudo-spin describing the two atomic contributions to the wave function. For our purpose here, we note that these linear bands are Dirac-like in which we can write the energy as

$$E = \pm\hbar v_F k \quad , \tag{3}$$

for which

$$v_F = \frac{3\gamma_0 a}{2\hbar} \tag{4}$$

is the effective "speed of light." One can use angle-resolved photo-emission data to check the energy value at M and K points [22], and this gives a value of γ_0 as 2.52±0.09 eV, and a Fermi velocity of 8.15±0.28 × 10^5 m/s. The second-neighbor interaction breaks the electron-hole symmetry around the Dirac point and we find a value of 0.083 eV for this parameter. Usually, however, one retains only the first-neighbor interaction and often takes γ_0 as 3 eV for convenience, which leads to a Fermi velocity of 9.7 × 10^5 m/s.

An important peculiarity of graphene is the Dirac band structure, which corresponds to particles with zero rest mass. That is, the effective mass of the particles at the Dirac point is exactly zero. Away from the Dirac point, the effective mass may be readily obtained by utilizing the equivalence of crystal momentum and quasi-particle momentum, as

$$m^* = \frac{\hbar k_F}{v_F} = \frac{\hbar}{v_F}\sqrt{\pi n} \quad , \tag{5}$$

a result that has been confirmed by cyclotron resonance studies [23]. In an equivalent fashion, the density of states, with both spin and valley degeneracy of 2, is given by

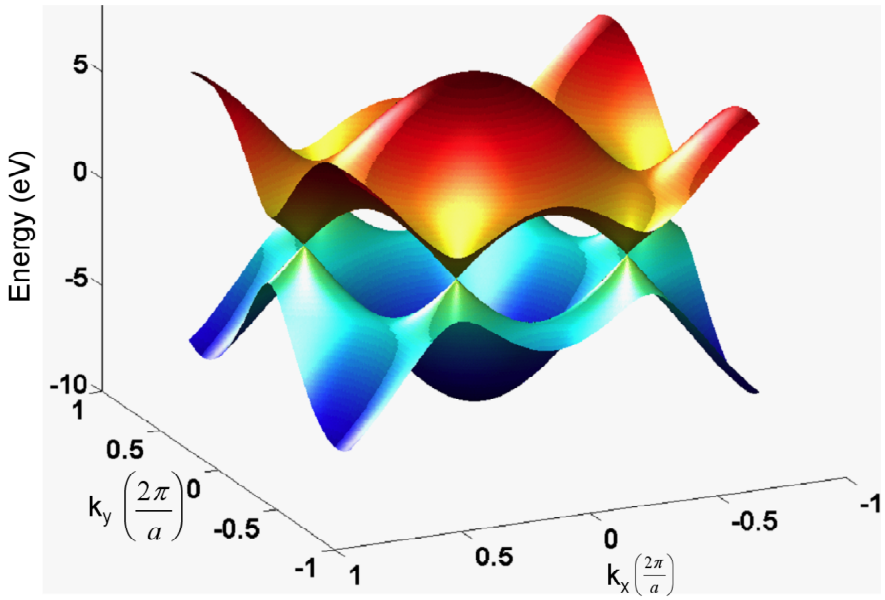

Fig. 2. The bandstructure of graphene [$\gamma_0 = 2.52$ eV, $\gamma_0' = 0.083$ eV, $E_0 = -0.25$ eV].

$$\rho(E) = \frac{2A}{\pi(\hbar v_F)^2} E \quad . \tag{6}$$

In intrinsic graphene, the Fermi level lies exactly at the Dirac point. The conductance does not go to zero at this point, but takes a value $\sim 4e^2/\pi h$ [24], which arises from quantum considerations of the zero bandgap. It has been reported that disorder in graphene can create electron-hole puddles, which cause an increase of the conductance at the Dirac point, as well as locally shift the Fermi energy from the Dirac point [25,26]. These puddles were proposed theoretically and have been observed experimentally [27,28]. The origin of the disorder remains an open question. In general, transport at room temperature is dominated by impurity scattering, where the impurities typically reside in the oxide upon which the graphene is placed. However, recent studies, in which a high-dielectric constant solvent has been placed around the graphene, has shown mobilities well above 40,000 cm^2/Vs [11], a value thought to be the intrinsic phonon limited mobility [12].

In bilayer graphene, one has the problem of arranging the two lattices with respect to each other. In general, these two layers are oriented in such a manner that the atoms of one sublattice in layer 1 are directly below the atoms of a sublattice in layer 2. The second set of atoms in layer 1 sit below the voids in the hexagons of layer 2. Still there arise two methods of stacking. In the Bernal stacking, the A atoms of layer 2 sit over the B atoms of layer 1 [29,30,31], but it has also been suggested that the A atoms of layer 2 sit over the A atoms of layer 1 [10,32]. Obviously these two differ only in the notation assigned to the atoms of layer 2. The major interaction, for band structure purposes, is between the two atoms sitting directly over one another, and this is denoted γ_1. Cyclotron resonance studies have given a value close to 0.43 eV for the electrons and 0.52 eV for the

holes [33] for this parameter, but a value of 0.39 also has been suggested [34]. Other interactions that

Fig. 3 A conceptual visualization of the separation of the entire system into a pair of leads plus the actual device.

have been considered are between the A atom of layer 1 and the next neighbor in layer 2 (γ_3) and between the two non-aligned atoms (γ_4).

3. The Recursive Green's Function Method

The Green's function has been applied to the study of small devices for a great many years. The most general formulation splits the overall system into three parts: a left contact, a right contact, and the active device under study, as can be seen in Fig. 3. Then, the total system Hamiltonian can be written in reduced block form as

$$H = \begin{bmatrix} H_L & H_{LD} & 0 \\ H_{DL} & H_D & H_{DR} \\ 0 & H_{RD} & H_R \end{bmatrix} . \tag{7}$$

The blocks labelled $H_{L(R)D}$ and their adjoints represent the coupling between the two contacts and the device itself. One example of this type of calculation is to study the structure of the oxide between a crystalline Si layer and a poly-Si layer [35]. It is usual to develop a coupling in which the contacts are reflected into the device Hamiltonian as self-energies, and conductance then developed from the reduced Hamiltonian for the device alone, as described by Fisher and Lee [36]. A modern approach to this is termed the *contact block reduction method* [37]. Nevertheless, this often still results is a Hamiltonian whose size is too large to effectively diagonalize. For this reason, the recursive Green's function (RGF) was developed [38,39]. This is easily generalized to include the effects of a magnetic field [40].

Before proceeding, however, it is worth making a comment. Many people claim to study transport with the non-equilibrium Green's functions (NEGF), but limit themselves to the ballistic case. When this is done, the lesser-than and greater-than correlation functions reduce to the normal retarded and advanced functions plus some self-energies which arise from interactions with the contacts [41,42], and the two Green's functions have their equilibrium form. The calculations here incorporate the same approach. While the NEGF are not specifically mentioned, any extension to non-ballistic transport would require the use of these two extra correlation functions, which can also be treated by recursive techniques.

3.1 The Slice Hamiltonian

The first step in applying the RGF method is to discretize the entire space of the nanostructure that is of interest. In the case of graphene, the atomic structure provides this discretization, and this is known as an atomic basis (as opposed to a lattice basis used in the case of known energy bands). Here, we assume a form for the e.g. left contact Green's function and then use this to connect to the

first slice of the device via a coupling interaction term, which is part of H_{LD}. It is only part of this term, as this latter term couples the left contact to the *entire* device, not just to the first slice. Hence, one part of the interation is to build up this overall interaction and the modification of the Green's function for the left contact, which we will denote as $G(0,0)$. To implement this, everything begins with the basic slice. In Fig. 4, we illustrate a small graphene quantum dot connected to two narrow ribbon leads. In this figure, we denote the basic slice for the case of zig-zag boundaries. The case for arm-chair boundaries can be done as easily [43,44], but we will stick to the former situation in this discussion. Each slice contains an equal number of *A* and *B* atoms. The graphene lattice itself is defined by three nearest-neighbor vectors, which are defined by

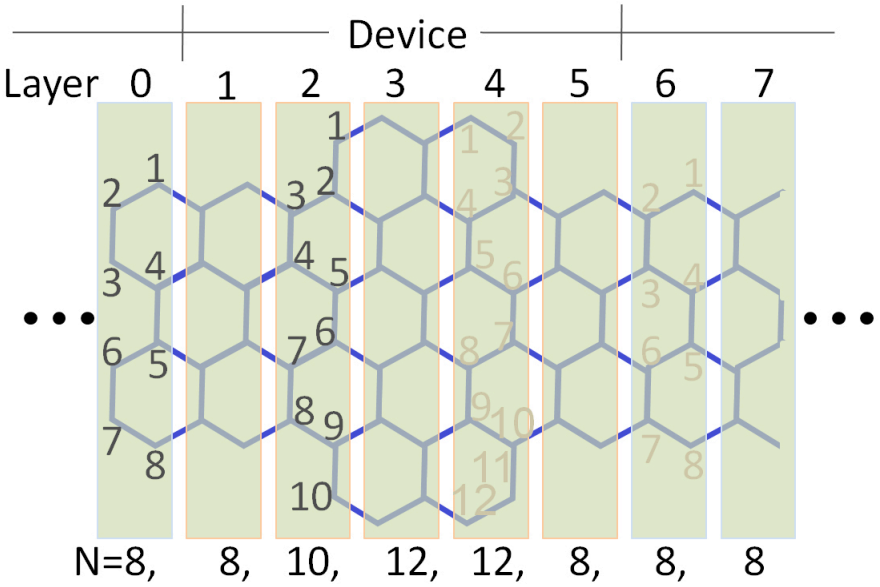

Fig. 4 The breakup of the overall system into a set of slices, some of which are denoted as contact slices.

$$\mathbf{d}_1 = a(0,-1) \quad , \quad \mathbf{d}_2 = \frac{a}{2}(\sqrt{3},1) \quad , \quad \mathbf{d}_3 = \frac{a}{2}(-\sqrt{3},1) \tag{8}$$

in the (x,y) plane, where a is the nearest neighbor distance of 0.142 nm. Let us consider slice 2, shown in Fig. 4, for example. The slice Hamiltonian for this slice is zero with the exception of the first off-diagonal terms. These terms have the nearest-neighbor coupling in these first off diagonal terms. If we have periodic lattices, then the description of the near-neighbor interactions includes the phase shifts that give rise to the Bloch sums. Here, however, we do not have this periodicity in either direction. Hence, the coupling terms in the interaction are merely the value of the overlap integral for wave functions on two adjacent atoms with the Hamiltonian. This is given the value

$$t_{i,i\pm1} = \gamma_0 \ . \tag{9}$$

When we consider bilayer graphene, we double the number of atoms in each slice, and pursue the more complicated inter-slice couplings that add off diagonal terms to the larger Hamiltonian for the slice.

The Hamiltonian which couples the slices is somewhat more complicated. Normally, on a rectilinear grid, this coupling Hamiltonian would be diagonal. Here, however, it is more difficult due

to the positions of the various atoms in the slice. Let us consider, for example, the coupling between slices 1 and 2 (the atoms designations are the same as for slice 0). Note from Fig. 4 that atom 1, in slice 1, is coupled to atom 3, in slice 2. Hence,

$$\left(H_{12}\right)_{1,3} = \gamma_0 \ . \tag{10}$$

By the same token, atom 4, in slice 1, is coupled to atom 4, in slice 2. This gives a diagonal term of the form

$$\left(H_{12}\right)_{4,4} = \gamma_0 \ . \tag{11}$$

It is important to note that this coupling Hamiltonian is not required to be Hermitian, as it is basically a self-energy term (only the total Hamiltonian is required to be Hermitian). One may be concerned about the lack of the phase shifts here, but we remind ourselves that the coupling is a simple two center integral. The basic structure of the interslice coupling Hamiltonians defines the crystal topology and this, together with the fact that all of the overlap integrals between nearest neighbors are equal, sets the nature of the atomic lattice, ensuring the hexagonal structure. Another important point in the interslice coupling term is that this Hamiltonian matrix is not square. Rather, we note that slice 1 and slice 2 have different numbers of atoms, so that the coupling Hamiltonian will have different numbers of rows and columns.

3.2 Adding a Magnetic Field

When an external magnetic field is applied, the hopping terms γ_0 discussed above acquire an additional phase due to the Peierls' phase factor. This additional phase factor is given by

$$\vartheta_{\mathbf{r},\mathbf{r}+\mathbf{d}} = 2\pi\phi_{\mathbf{r},\mathbf{r}+\mathbf{d}} / \phi_0 \ , \tag{12}$$

where $\phi_0 = h/e$ is the flux quantum. The coupled flux is given by

$$\phi_{\mathbf{r},\mathbf{r}+\mathbf{d}} = \int_{\mathbf{r}}^{\mathbf{r}+\mathbf{d}} \mathbf{A}\cdot\mathbf{dr} \ . \tag{13}$$

In this expression, **d** is any of the three nearest-neighbor vectors that appear in (9), and the full x and y shift from one atom to the next must be included. Typically, however, one uses the Landau gauge in which $\mathbf{A} = (-By,0)$, so that only the x shift is incorporated, although the y position directly affects the amount of that phase shift. Hence, by the time one has moved across the slice, the entire flux through the slice has been incorporated. Generally, however, one evaluates the y value at points midway between the two atoms being coupled.

An important point with the magnetic field in structures in which the slices may have different extent in the transverse direction is the position of $y = 0$. This needs to be at the center of the slice, so that there is no discontinuity in the vector potential as one moves from one slice to the next.

3.3 The Recursive Procedure

The recursion begins by establishing a self-energy correction which acts upon the first slice, but is based upon the left contact and its connection to the first slice. That is, we define the left self-energy by the action

$$\Sigma_L = H_{10}G_{00}H_{01} \quad , \quad \Gamma_L = i\left(\Sigma_L - \Sigma_L^+\right) \ , \tag{14}$$

where

$$G_{00} = \left(EI - H_0 + i\eta\right)^{-1} \ , \tag{15}$$

and a small damping factor has been added for convergence purposes. Here, I is a unit matrix and E is the Fermi energy. We then recompute the Green's function for the 0th slice to be

$$G(0,0) = \left(EI - H_0 + \Sigma_L + i\eta\right)^{-1} \ . \tag{16}$$

We now can propagate across the structure using the recursion for $j > 1$ as

$$G(j,j) = \left(EI - H_j - H_{j,j-1}G(j-1,j-1)H_{j-1,j}\right)^{-1} \quad . \tag{17}$$

But, we will also need another Green's function in order to compute the transmission, and this is found from the auxiliary functions

$$\begin{aligned} G(0,j) &= G(0,j-1)H_{j-1,j}G(j,j) \\ G(j,0) &= G(j,j)H_{j,j-1}G(j-1,0) \end{aligned} \quad . \tag{18}$$

At the right contact, we have to connect to the boundary. Let us assume that the last device slice has $s = L$, then the right contact Green's functions become

$$\begin{aligned} G(L+1,L+1) &= \left(EI - H_R + \Sigma_R - H_{L+1,L}G(L,L)H_{L,L+1}\right)^{-1} \\ G(0,L+1) &= G(0,L)H_{L,L+1}G(L+1,L+1) \\ G(L+1,0) &= G(L+1,L+1)H_{L+1,L}G(L,0) \end{aligned} \quad . \tag{19}$$

Here, the right self-energy has been computed in exactly the same manner as (14), but with the right contact Hamiltonian. The transmission through the total system is now found from (one doesn't worry about the velocities since they are all equal to the Fermi velocity)

$$T = Tr\left\{\Gamma_L G(0,L+1)\Gamma_R G^{+}(L+1,0)\right\} \quad . \tag{20}$$

In many cases, one also wants to know the reflection coefficient, in order to make sure that flux is conserved in the system. In this case, one needs to also compute the interaction of the entire system on the Green's function for the left contact. Hence, we need an additional recursion

$$G(0,0) = G(0,0) + G(0,j-1)H_{j-1,j}G(j,0) \quad . \tag{21}$$

The reflection coefficient is then essentially the trace of the squared magnitude of $G(0,0)$.

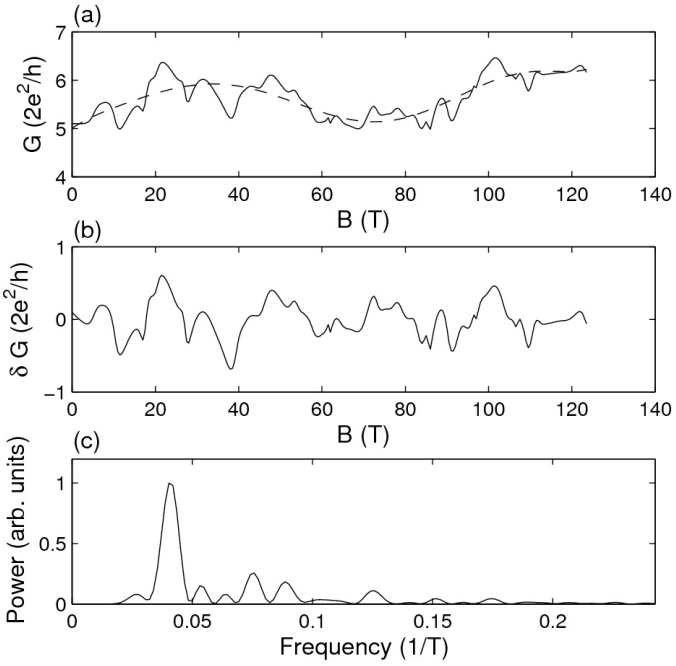

Fig. 5 (a) Conductance through a 20 nm square graphene quantum dot with 4 nm leads. (b) The conductance fluctuations after the background (slowly varying conductance shown as the dashed line in (a)) is removed. (c) Fourier spectrum of the conductance fluctuations showing that a single dominant frequency governs the fluctuations.

The charge density may be found at each atomic site by utilizing the slice Green's function $G(j,j)$. In much the same way that the density of states is found, we find the probability density, at the Fermi energy, at site i in slice j to be

$$\rho_{ij} = -\frac{1}{\pi}\mathrm{Im}\left\{\left[G(j,j)\right]_{ii}\right\} . \tag{22}$$

To find the total density, we need to integrate over all energies up to the Fermi energy (measured from zero for the electrons). This is usually a integral sensitive to energy gridding, and a contour along a complex energy is often used to ease this problem.

3.4 An Example

As an example, we compute the conductance through a 20 × 24 nm square graphene, single layer quantum dot, in which leads of 4 nm width are applied. In Fig. 5, we plot the total conductance, the fluctuations after the background has been subtracted and the Fourier spectra of these fluctuations. Here, the so-called background that is subtracted is found by smoothing the overall curve. The tunnelling to the pointer states gives rise to Fano resonances, and these can be smoothed away to yield the background conductance. In experiment, the procedure is usually to raise the temperature to a few degrees, where the fluctuations are heavily damped and this curve used for the subtraction. The spirit is the same, as the smoothing gives an effective temperature effect. For reasons that will become clear in the next section, the magnetic field is rather high, but it is clear that a single narrow band of frequencies dominate the fluctuations. This is in keeping with the results found on normal semiconductor quantum dots in which the set of pointer states, and their periodic reappearance at particular magnetic fields corresponds to the existence of quantum Darwinism in this system [9].

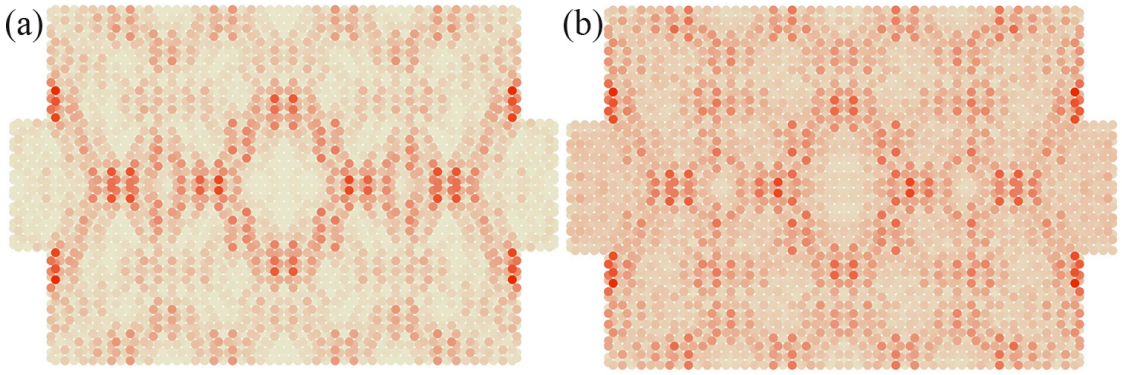

Fig.6 (a) One of the eigenstates of a closed dot. (b) A pointer state found in the open dot at the same energy as that of the state in (a).

Another interesting aspect is the comparison between the eigenstates of the closed system, which can be computed by diagonalizing the full Green's function determined from the Hamiltonian (7) and the pointer states which remain in the open system, which are computed from the density at each atomic site found from the Green's function. In Fig. 6, we show results for a rectangular shaped dot, and compare one eigenstate found in the closed dot with a pointer state found in the open dot. The agreement between these two results clearly shows the connection between the pointer states and the eigenstates, and that the latter are states which have not undergone decoherence.

4. Scaling in Quantum Dots

In this section, we would like to examine how the dominant frequency of the fluctuation, as seen in Fig. 5(c), varies with dot size. In general, these fluctuations, due to phase space tunnelling to the pointer states, only occur in the low magnetic field regime [45]. Once the cyclotron radius fits within the dot, then edge states begin to form, and the transport is dominated by the quantum Hall effect. Consequently, we need to scale the magnetic field with the dot size. In general, we can develop the scaling factor for the maximum of the magnetic field by setting the dot size D equal to the cyclotron radius at the Fermi energy, as

$$D = l_B^2 k_F \ , \tag{23}$$

where

$$l_B = \sqrt{\frac{\hbar}{eB}} \tag{24}$$

is the magnetic length. The Fermi wavelength is found from the Dirac band energy $E = \hbar v_F k_F$, with the Fermi velocity being given by (4). Then, we find that the scaling is given by

$$D = \frac{2\hbar(E/\gamma_0)}{3eaB} \ , \tag{25}$$

or the maximum magnetic field is given by

$$B_{\max} = \frac{2\hbar(E/\gamma_0)}{3eaD} \ . \tag{25a}$$

We follow this scaling in the range of magnetic field that is studied in the set of dots that we examine.

Here, we will examine single layers of graphene, using $\gamma_0 = 3$, as well as bilayers of graphene. For the bilayers, we assume the Bernal stacking with parameters $\gamma_0 = 3.16$, $\gamma_1 = 0.39$ and $\gamma_3 = 0.315$ [34]. Here, γ_1 represents the coupling between the two aligned A and B' atoms of the first and second layers. The other constant represents the coupling between the nonaligned B (in the center of the hexagon) and A' atoms of the second layer. In Fig. 7, we show a sketch of the 20 nm dot and its leads. For dot sizes W = 20-50 nm, we will use a 4 nm lead width and an energy of $E/\gamma_0 = 0.8$. For larger dots, the lead opening is scaled up as $4(W/50)$ nm and the energy is reduced as $E/\gamma_0 = 0.8(50/W)$. The fluctuations for the smallest dot, for graphene, is shown in Fig. 5(a). The fluctuations for the bilayer dot are quite similar, and we compare these in Fig. 8. Our interest is in the dominant frequency of the fluctuations, and we summarize the results for a series of dots in Fig. 9.

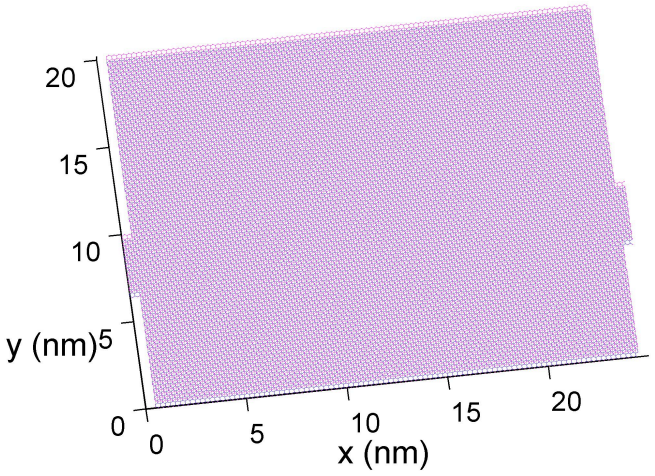

Fig. 7 A schematic drawing of the bilayer graphene quantum dot, showing the connection of the two leads.

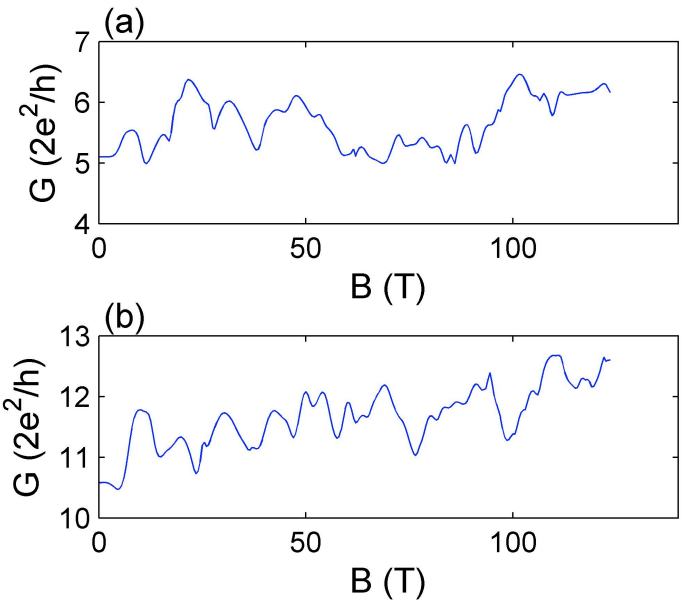

Fig. 8 Fluctuations observed in a single graphene layer dot (a) and in a bilayer dot (b).

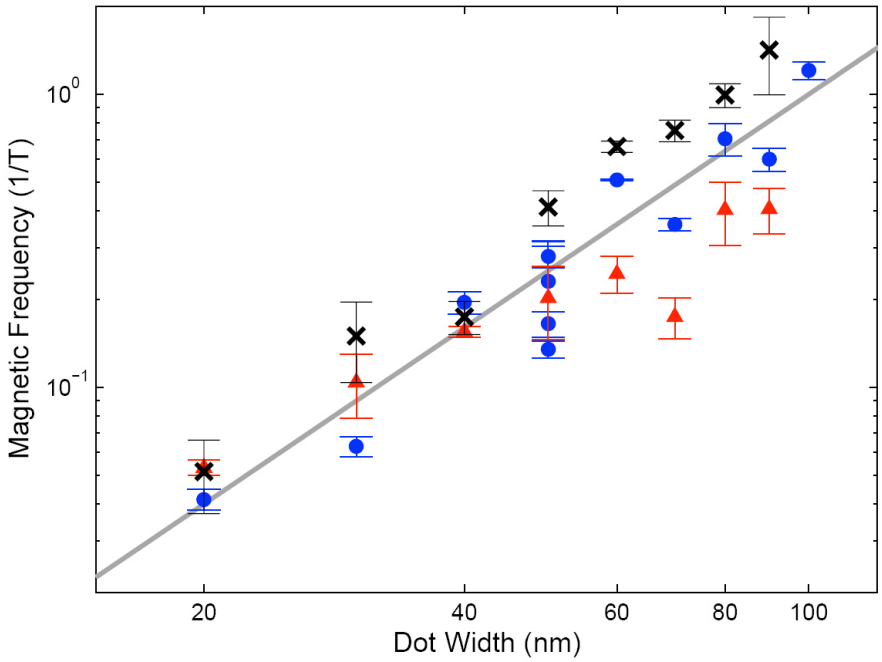

Fig. 9 The variation of the dominant magnetic frequency with the dot size. The monolayer graphene is plotted as solid circles while the bilayer graphene is plotted with the triangles. Bilayer graphene with a factor of 2 lower energy is plotted as the crosses. It is not clear whether or not a real difference exists between the various results.

There is a clear change in behavior as the size of the dot increases beyond ca. 50 nm. For smaller dot sizes, the magnetic frequency is largely the same in both the monolayer and bilayer dots. However, for the larger dots, the two frequencies clearly diverge. Recent experiments in a much larger quantum dot in bilayer graphene suggests a magnetic frequency of about 9 T^{-1} at a dot size of 0.5 μm [20]. Scaling of the single layer graphene data in Fig. 9 to this size would suggest a magnetic frequency 2-3 times as large. There is insufficient data in the figure to estimate whether the bilayer data would extrapolate to a value near that observed, but it is certain that the bilayer would likely have a much lower magnetic frequency. We can only hope that, as we examine larger dots, we can extend these curves to a size that matches that used in the experiment.

It is also worth noting that there is no obvious power law relationship between the dot size and the magnetic frequency in Fig. 9, although the solid line represents a scaling with the area of the dot. In previous studies of dot size in semiconductor dots, experiments on dots in the range of 0.7-1.2 μm on a side showed a scaling with the dot edge size [46,47]. Simulations, however, exhibited multiple frequencies in these large dots and a transition from behavior in which the magnetic frequency scaled with the dot area in smaller dots [48], typically with an edge less than 300 nm in extent. If we take all the curves together in Fig. 9, then it appears that scaling with the dot area seems to be appropriate for these small dots, as was found in the semiconductor dots. One point worth noting is that if we extend the solid curve in Fig. 9 to a dot size commensurate with the recent experiments [20], then the expected frequency is approximately 9 T^{-1}, which is the value found in the experiments.

5. Conclusions

Here, we have examined the nature of fluctuations in quantum dots at low magnetic fields, in which transport is thought to exhibit phase space tunneling to pointer states within the dots. These fluctuations are seen in graphene, with its "relativistic" massless Dirac band structure, just as in semiconductor quantum dots, with similar characteristic features at similar sizes. The use of the recursive Green's function method, with an atomic basis set by the individual atoms of graphene, captures the important aspects of the transport and fluctuations, and remains an important tool for studies of transport in a wide range of mesoscopic structures.

The authors would like to thank S. M. Goodnick, R. S. Shishir, and I. Knezevic for many helpful discussions.

[1] Wheeler J A, Zurek W H, *Quantum Theory and Measurement* (Princeton University Press, Princeton, N. J., 1983).
[2] Ketzmerick R, *Phys. Rev. B* **54**, 10841 (1996).
[3] Zurek W H, *Rev. Mod. Phys.* **75**, 715 (2003).
[4] Ferry D K, Akis R, Bird J P, *Phys. Rev. Lett.* **93**, 026803 (2004).
[5] Ferry D K, Akis R, Bird J P, *J. Phys. Cond. Matt.* **17**, S1017 (2005).
[6] Broer H W, *Bull. Amer. Math. Soc.* **41**, 507 (2004).
[7] de Moura A P S, Lai L-C, Akis R, Bird J P, Ferry D K, *Phys. Rev. Lett.* **88**, 236804 (2002).
[8] Brunner R, Meisels R, Kuchar F, Akis R, Ferry D K, Bird J P, *Phys. Rev. Lett.* **98**, 204101 (2007).
[9] Brunner R, Akis R, Ferry D K, Kuchar F, Meisels R, *Phys. Rev. Lett.* **101**, 024102 (2008).
[10] Castro Neto A H, Guinea F, Peres N, Novoselov K S, Geim A, *Rev. Mod. Phys.* **81,** 109 (2009).
[11] Chen F, Xia J, Ferry D K, Tao N J, *Nano Lett.* **9**, 2571 (2009).
[12] Shishir R S, Ferry D K, *J. Phys. Cond. Matt.* **21**, 232204 (2009).
[13] Silvestrov P G, Efetov K B, *Phys. Rev. Lett.* 98, 016802 (2007).
[14] Pereira J M, Jr., Vasilopoulos P, Peeters F M, *Nano Lett.* 7, 946 (2007).

[15] Stampfer C, Güttinger J, Molitor F, Graf D, Ihn T, Ensslin K, *Appl. Phys. Lett.* **92**, 012102 (2008).
[16] Ponomarenko L A, Schedin F, Katsnelson M I, Yang R, Hill E W, Novoselov K S, Geim, A K, *Science* **320**, 356 (2008).
[17] Libisch F, Stampfer C, Burgdörfer J, *Phys. Rev. B* **79**, 115423 (2009).
[18] Huang L, Lai Y-C, Ferry D K, Goodnick S M, Akis R, *Phys. Rev. Lett* **103**, 054101 (2009).
[19] Huang L, Lai Y-C, Ferry D K, Akis R, Goodnick S M, *J. Phys. Cond. Matt.* **21**, 344203 (2009).
[20] Ujiie Y, Morimoto T, Aoki N, Ferry D K, Bird J P, Ochiai Y, *J. Phys. Cond. Matt., in press*.
[21] Wallace P R, *Phys. Rev.* **71**, 622 (1947).
[22] Bostwick A, Ohta T, Seyller T, Horn K, Rotenberg E, *Nature Phys.* **3**, 37 (2006).
[23] Novoselov K S, Geim A, Morozov S V, Jiang D, Katsnelson M I, Grigorieva I V, Dubonos S V, Firsov A A, *Nature* **438**, 197 (2005); Bostwick A, Ohta T, Seyller T, Horn K, Rotenberg E, *Nature Phys.* **3**, 37 (2006).
[24] Fradkin E, *Phys. Rev. B* **33**, 3257 (1986); Ludwig A, Fisher M, Shankar R, Grinstein G, *Phys. Rev. B* **50**, 7526 (1994); Aleiner I L, Efetov K B, *Phys. Rev. Lett.* 97, 236801 (2006); Atland A, *Phys. Rev. Lett.* **97**, 236802 (2006); Peres N M, Guinea F, Castro Neto A H, *Phys. Rev. B* **73**, 125411 (2006); Fritz L, Schmalian J, Müller M, Sachdev S, *Phys. Rev. B* **78**, 085416 (2008); Kashuba A, *Phys. Rev. B* **78**, 085415 (2008); Bardarson J H, Tworzydło J, Brouwer P W, Beenakker C W J, *Phys. Rev. Lett.* **99**, 106801 (2007).
[25] Rossi E, Das Sarma S, *Phys. Rev. Lett.* **101**, 166803 (2008).
[26] Katsnelson M I, Novoselov K S, Geim A K, *Nature Phys.* **2**, 620 (2006).
[27] Hwang E H, Adam S, Das Sarma S, *Phys. Rev. Lett.* **98**, 186806 (2007).
[28] Martin J, Akerman N, Ulbricht G, Lohmann T, Smet J H, von Klitzing K, Yacoby A, *Nature Phys.* **4**, 144 (2008).
[29] McCann E, Falko V I, *Phys. Rev. Lett.* **96**, 086805 (2006).
[30] Castro E V, Novoselov K S, Morozov S V, Peres N M R, Lopes dos Santos J M B, Nilsson J, Guinea F, Geim A K, Castro Neto A H, *Phys. Rev. Lett.* 99, 216802 (2007).
[31] Park C-H, Giustino F, Cohen M L, Louie S G, Nano Lett. 8, 4229 (2008).
[32] Li Z Q, Henriksen E A, Jiang Z, Hao Z, Martin M C, Kim P, Stormer H L, and Basov D N, *Phys. Rev. Lett.* 102, 037403 (2009).
[33] Henriksen E A, Jiang Z, Tung L-C, Schwartz M E, Takita M, Wang Y-J, Kim P, Stormer H L, *Phys. Rev. Lett.* **100**, 087403 (2008).
[34] Koshino M, Ando T, *Phys. Rev. B* **73**, 245403 (2006).
[35] Demkov A A, Zhang X, Drabold D A, *Phys. Rev. B* **64**, 125306 (2001).
[36] Fisher D S, Lee P A, *Phys. Rev. B* **23**, 6851 (1981).
[37] Mamaluy D, Vasileska D, Sabathil M, Zibold T, Vogl P, *Phys. Rev. B* **71**, 245321 (2005).
[38] Lee P A, Fisher D S, *Phys. Rev. Lett.* **47**, 882 (1981).
[39] Thouless D J, Kirkpatrick S, *J. Phys. C* **14**, 235 (1981).
[40] Ando T, *Phys. Rev. B* **44**, 8017 (1991).
[41] Meir Y, Wingreen, N S, *Phys. Rev. Lett.* **68**, 2512 (1992).
[42] Ferry D K, Goodnick, S M, Bird, J P, *Transport in Nanostructures*, 2nd Ed. (Cambridge Univ. Press, 2009) Sec. 9.4.4.
[43] Wakabayashi K, Fujita M, Ajiki H, Sigrist M, *Phys. Rev. B* **59**, 8271 (1999).
[44] Li T C, Lu S-P, *Phys. Rev. B* **77**, 085408 (2008).
[45] Akis R, Bird J P, Vasileska D, Ferry D K, de Moura A P S, Lai Y-C, in *Electron Transport in Quantum Dots*, Ed. by Bird J P (Kluwer, Boston, 2003) 209-276.

[46] Bird J P, Ishibashi, K, Aoyagi Y, Sugano T, Akis R, Ferry D K, Pivin D P Jr., Connolly K M, Taylor R P, Newbury R, Olatona D M, Micolich A, Wirtz R, Ochiai Y, Okubo Y, *Chaos Sol. & Fractals* **8**, 1299 (1997).
[47] Ferry D K, Bird J P, Akis R, Pivin D P, Jr., Connolly K M, Ishibashi K, Aoyagi, Y, Sugano T, Ochiai Y, *Jpn. J. Appl. Phys.* **36**, 3944 (1997).
[48] Holmbert N, Akis R, Pivin D P Jr., Bird J P, Ferry, D K, *Semicond. Sci. Technol.* **13**, A21 (1999).